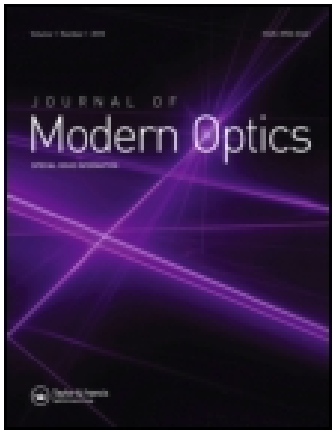

Journal of Modern Optics

Publication details, including instructions for authors and subscription information:
http://www.tandfonline.com/loi/tmop20

Nonlocal nonlinear refractive index of gold nanoparticles synthesized by ascorbic acid reduction: comparison of fitting models

A. Balbuena Ortega[a], M.L. Arroyo Carrasco[a], M.M. Méndez Otero[a], V.L. Gayou[b], R. Delgado Macuil[b], H. Martínez Gutiérrez[c] & M.D. Iturbe Castillo[d]

[a] Facultad de Ciencias Físico-Matemáticas, Benemérita Universidad Autónoma de Puebla, Av. San Claudio y 18 Sur. Col. San Manuel, C.P. 72570, Puebla, Puebla, México

[b] CIBA-IPN Tlaxcala, Km. 1.5 Carretera Estatal Tecuexcomac-Tepetitla, C.P. 90700, Tepetitla de Lardizabal, Tlaxcala, México

[c] CNMN-IPN, Calle Luis Enrique Erro s/n, Unidad Profesional Adolfo López Mateos, Col. Zacatenco, C.P. 07738 DF, México

[d] Instututo Nacional de Astrofísica Óptica y Electrónica, Luis Enrique Erro # 1, C.P. 72840 Tonantzintla, Puebla, México

Published online: 21 Aug 2014.

To cite this article: A. Balbuena Ortega, M.L. Arroyo Carrasco, M.M. Méndez Otero, V.L. Gayou, R. Delgado Macuil, H. Martínez Gutiérrez & M.D. Iturbe Castillo (2014) Nonlocal nonlinear refractive index of gold nanoparticles synthesized by ascorbic acid reduction: comparison of fitting models, Journal of Modern Optics, 61:sup1, S67-S72

To link to this article: http://dx.doi.org/10.1080/09500340.2014.950621

Journal of Modern Optics, 2014
Vol. 61, No. S1, S67–S72, http://dx.doi.org/10.1080/09500340.2014.950621

Nonlocal nonlinear refractive index of gold nanoparticles synthesized by ascorbic acid reduction: comparison of fitting models

A. Balbuena Ortega[a]*, M.L. Arroyo Carrasco[a], M.M. Méndez Otero[a], V.L. Gayou[b], R. Delgado Macuil[b], H. Martínez Gutiérrez[c] and M.D. Iturbe Castillo[d]

[a]*Facultad de Ciencias Físico-Matemáticas, Benemérita Universidad Autónoma de Puebla, Av. San Claudio y 18 Sur. Col. San Manuel, C.P. 72570, Puebla, Puebla, México;* [b]*CIBA-IPN Tlaxcala, Km. 1.5 Carretera Estatal Tecuexcomac-Tepetitla, C.P. 90700, Tepetitla de Lardizabal, Tlaxcala, México;* [c]*CNMN-IPN, Calle Luis Enrique Erro s/n, Unidad Profesional Adolfo López Mateos, Col. Zacatenco, C.P. 07738 DF, México;* [d]*Instututo Nacional de Astrofísica Óptica y Electrónica, Luis Enrique Erro # 1, C.P. 72840 Tonantzintla, Puebla, México*

(*Received 11 March 2014; accepted 28 July 2014*)

In this paper, the nonlinear refractive index of colloidal gold nanoparticles under continuous wave illumination is investigated with the *z*-scan technique. Gold nanoparticles were synthesized using ascorbic acid as reductant, phosphates as stabilizer and cetyltrimethylammonium chloride (CTAC) as surfactant agent. The nanoparticle size was controlled with the CTAC concentration. Experiments changing incident power and sample concentration were done. The experimental *z*-scan results were fitted with three models: thermal lens, aberrant thermal lens and the nonlocal model. It is shown that the nonlocal model reproduces with exceptionally good agreement; the obtained experimental behaviour.

Keywords: nonlocal nonlinear response; *z*-scan; gold nanoparticles

1. Introduction

Considerable attention has recently been given to nonlinear optical properties of nanosized metal particles because of their strong and size-dependent plasmon resonance absorption [1]. Metal nanoparticles are of special interest to optics as nonlinear materials due to their large third-order nonlinearity (χ^3) and ultrafast response time [2]. The enhanced optical nonlinearity in metal nanoparticles was known to stem from the high amplification of local electric field near to the metal particles at the surface plasmon resonance (SPR) frequency [3], the nonlinear optical response has been attributed to electronic and thermo-optical effects. Several works have reported *z*-scan curves of samples of metal nanoparticles, and these results have been fitted using different models. For example, in [4], samples of gold nanoparticles were fitted with the Sheik-Bahae model [5], [6]; in [7], samples of silver nanoparticle colloids were fitted with the thermal lens model [8], [18]; in [9], samples of silver nanoparticles were fitted with the aberrant lens model [10]; samples of copper nanoparticles were fitted using the numerical solution of an integral equation (Equation (12) in Ref. [11]). Although such models provide, for particular cases, good fitting to the experimental results they do not fit for the general case, because as was proved in reference [12], models based in parabolic approximations are not adequate, in this reference, a comparison between different models was presented and a *z*-scan general theory considering only the local case was proposed.

A phenomenological model that takes into account the nonlocal character of the nonlinear optical response of a thin media illuminated with a Gaussian beam in the *z*-scan technique was proposed in reference [13]. In this model, the nonlocal feature of the nonlinear response is considered as a parameter *m*, which modifies the transverse spatial extension of the photoinduced phase change of the light beam at the output face of the nonlinear sample [14]. With this model, it was possible to reproduce qualitatively experimental results reported for gold nanoparticles in cyclohexanone, under CW radiation at 532 nm, and large magnitude of the on-axis nonlinear phase change [13].

In this work, it is investigated, the nonlocal nonlinear optical response of colloidal gold nanoparticles synthesized by ascorbic acid reduction using cetyltrimethylammonium chloride (CTAC), as surfactant agent, which allows a control of nanoparticles size. *z*-scan curves are obtained for different concentrations of CTAC and the experimental data are fitted with three models; thermal lens [8], [15], aberrant thermal lens [10], [15] and the general nonlocal model proposed in reference [13]. It is shown that the nonlocal model provides a better fitting to the experimental results.

*Corresponding author. Email: abalbuena1984@gmail.com

2. Nanoparticles synthesis

The synthesis of gold nanoparticles was carried out using ascorbic acid as reductant, phosphates as stabilizer and CTAC as surfactant agent. High-purity water with a resistivity of 18 MΩcm was used in all the experiments. Stock solutions of ascorbic acid (2 mM), tribasic phosphate (1 mM), $HAuCl_4$ (1 mM) and CTAC (1 mM) were prepared in 50 ml aqueous solution. The stock solutions were used few days after their preparation to obtain the samples. The phosphate solutions (1 ml) were first mixed with 1 ml of gold salts and stirred for 15 min. CTAC with concentrations of: 100 µl (sample A), 200 µl (sample B), 400 µl (sample C), 600 µl (sample D), 800 µl (sample E) and 1000 µl (sample F) were subsequently added and stirred for 15 min, finally 600 µl of ascorbic acid solution was added in order to develop stable nanoparticle solutions in few seconds.

UV–vis spectra of synthesized nanoparticle solutions were obtained with a Thermo spectrophotometer (Evolution 600). As reported in [16], the simultaneous mixing of the tetrachloroauric acid and ascorbic acid solutions results in a fast formation of stable gold nanoparticle solutions. The addition of CTAC slows the reaction velocity which allows to control the nanoparticles size. In Figure 1, the UV–vis absorption spectra of samples obtained with different concentrations of CTAC are shown. As the concentration of CTAC is increased the SPR band is shifted to shorter wavelengths, a region which is associated to a decrease in the particle size. At lower concentrations (samples A, B and C), the SPR band is broad due to the formation of polydisperse particles [17], see Figure 2(*a*). When the quantity of CTAC is increased (samples D, E and F), the SPR band becomes narrower which is a characteristic of monodisperse particles, see Figure 2(*b*). The results show that this surfactant (CTAC) limits the agglomeration of particles and then controls the particle size. The explanation of this effect is the role that CTAC plays in the passivation of formed gold nanoparticles. High CTAC concentration allows the stabilization of smaller particles while for low concentration, the coverage is incomplete and a coarsening process leads to aggregation of large entities. The nanoparticle sizes of the different samples were obtained from SEM images, see Table 1.

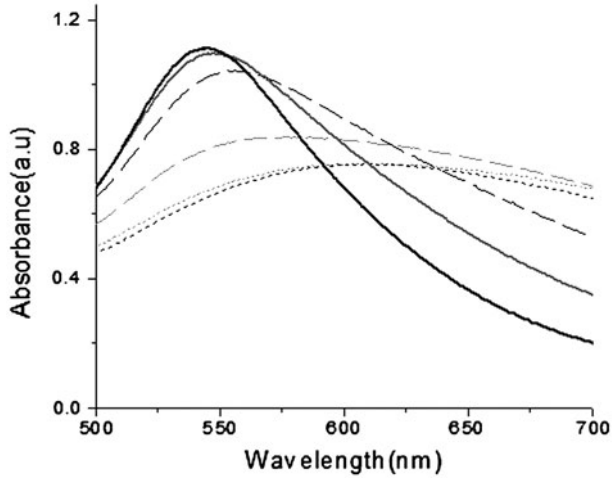

Figure 1. UV–vis absorption spectra for samples: A (dotted grey line), B (dotted black line), C (dashed grey line), D (dashed black line), E (solid grey line) and F (solid black line).

3. Nonlocal model

Remarkable differences in the far-field intensity patterns and the *z*-scan curves can be obtained in thin nonlinear media, illuminated by a Gaussian beam, depending on its degree of nonlocality. When the photoinduced refractive index change profile is bigger or smaller than the incident intensity profile, the nonlinear medium is regarded as nonlocal. The model, established in [13], considers a Gaussian beam of wavelength λ, with field amplitude $E(r, z)$, propagating in the *z*-direction. This beam illuminates a thin nonlinear sample set at z distance from the waist. The output field E_{out} after the thin medium is given by;

$$E_{\text{out}} = E(r,z)\exp(-i\Delta\phi(r)), \tag{1}$$

where $\Delta\phi(r)$ is the nonlinear phase change, that for a general nonlocal media is given by [13]:

$$\Delta\phi(r) \approx \Delta\phi_0(z,m)\exp(-mr^2/w(z)^2), \tag{2}$$

where

$$\Delta\phi_0(z,m) = \frac{\Delta\Phi_0}{(1+(z/z_0)^2)^{m/2}}, \tag{3}$$

here, $\Delta\Phi_0$ is the maximum on-axis photoinduced phase shift of the beam when the nonlinear medium is placed at $z = 0$, z_0 is the Rayleigh distance of the beam and m can be any real positive number. The locality or nonlocality of the nonlinear response is implied in the m parameter. Only for $m = 2$ (local case) the nonlinear phase change follows the incident intensity distribution. In order to obtain the far-field on-axis intensity, the Fourier transform of the output field, Equation (1), was obtained numerically for a given value of $\Delta\Phi_0$ and the m parameter. *z*-scan curves were obtained with these on-axis intensity data for different positions of the thin sample.

4. z-scan experimental results

In this work, the nonlinear optical properties of the colloids were investigated with the *z*-scan technique using an Argon ion laser beam with a wavelength of 514 nm, and power up to $p = 40$ mW. The laser beam was

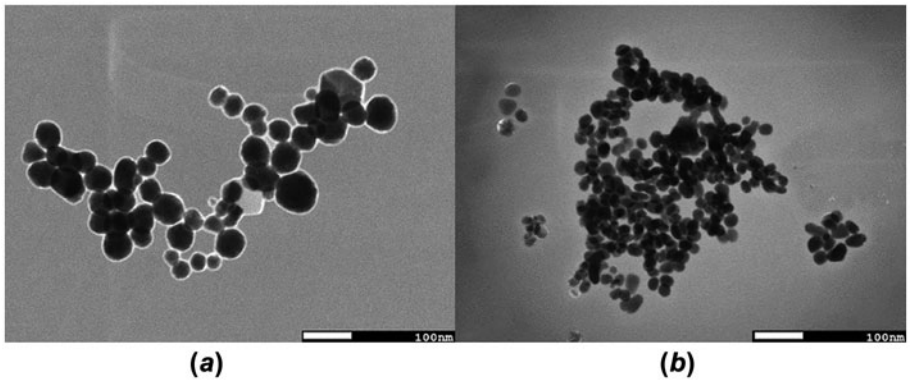

Figure 2. SEM image of the gold nanoparticles for sample A (*a*) and sample F (*b*).

Table 1. CTAC concentration, absorbance peak position and nanoparticle size of the different samples.

	CTAC (μl)	Absorbance peak position (nm)	Nanoparticle size (nm)
A	100	608	50 ± 15
B	200	604	48 ± 14
C	400	580	41 ± 12
D	600	556	35 ± 11
E	800	549	31 ± 9
F	1000	547	25 ± 7

focused onto the sample by a convergent lens with a focal length of 3.5 cm, generating a beams waist of 15 μm. The nonlinear medium was confined in a 1 mm width quartz cell. This cell was mounted on a translation stage and moved in the on-axis direction around the lens focus by a computer-controlled servo motor. The transmitted light through on-axis small aperture (1 mm radius), was measured at far field by a photodetector located 1 m away of the lens, as a function of the sample position, to obtain the closed-aperture *z*-scan. The experimental open-aperture *z*-scan curves of this type of samples did not demonstrate any nonlinear absorption contribution.

In Figure 3, the experimental results obtained for the normalized closed-aperture *z*-scan curves for the sample with higher concentration of CTAC (F sample) using different incident laser powers: 2.5 mW (*), 8 mW (□), 16 mW (+) and 40 mW (o) are shown. The obtained *z*-scan curves were asymmetric, exhibited a negative nonlinear refractive index and the amplitude of the *z*-scan curves grew with the incident power. The Δz_{p-v} values range from 3.0 to 3.3 mm (2.2–2.4 z_0), and the ΔT_{p-v} values range from 0.3 to 4. These *z*-scan curves are not typical for a Kerr local media: (z_{p-v} is larger than the expected value and the largest amplitude of the *z*-scan curve did not present some oscillations in the minima [12].

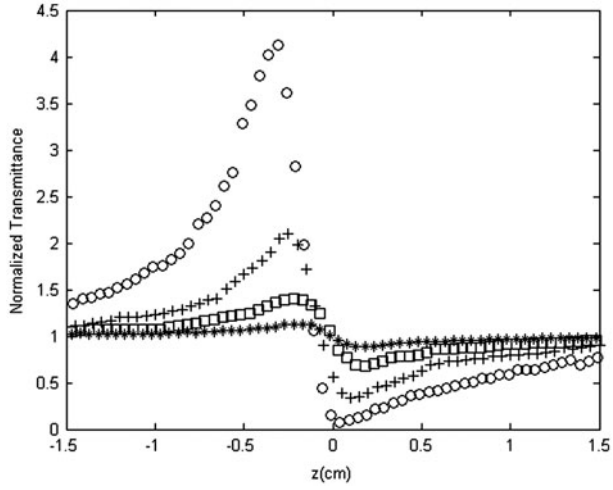

Figure 3. Experimental *z*-scan curves for the F sample with an incident laser power of: 2.5 mW (*), 8 mW (□), 16 mW (+) and 40 mW (o).

In Figure 4, the *z*-scan curves obtained for the different samples under the same incident power of 16 mW are shown. As we can see, the amplitude of the *z*-scan curve grows with the concentration of CTAC. The *z*-scan curve are asymmetric; the amplitude of the peak is larger than the valley.

5. Comparison of models

In this section, our experimental results are compared with different models used to fit experimental results for similar samples under similar experimental conditions. Although models exist that consider *z*-scan curves obtained for a thin media under particular experimental conditions can contain contributions from different physical mechanisms, for example [18], however, such models were not considered here because we assume that the nonlinear response exhibited by our samples was of one

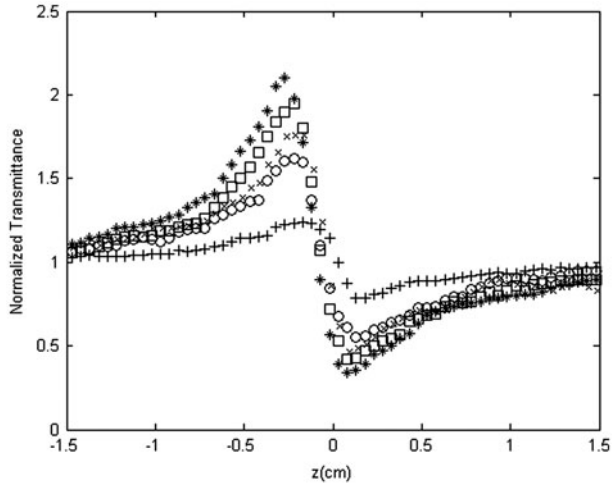

Figure 4. Experimental z-scan curves for an incident power of 16 mW and samples with different CTAC concentrations: Sample B (+), Sample C (o), Sample D (×), Sample E (□) and Sample F (*).

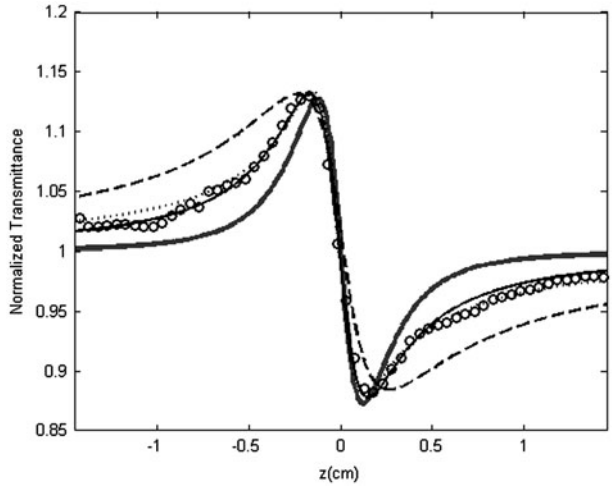

Figure 5. Experimental (o) and calculated z-scan curves for the F sample with incident power of 2.5 mW. Fitting with the: Sheik-Bahae model (grey line), thermal lens model (dashed line), aberrant thermal lens model (dotted line) and the nonlocal model (black line) of Ref. [13].

type. First, we compare with the thermal lens model where the normalized transmittance of the z-scan is given by [10]:

$$T = \left[1 + \frac{2\theta_{TL}x}{1+x^2} + \frac{\theta_{TL}^2}{1+x^2}\right]^{-1}, \quad (4)$$

where θ_{TL} is the fitting parameter (for us) and $x = z/z_0$. This expression is valid for steady-state conditions.

As a second model to compare our results, we use the aberrant thermal lens model where the normalized transmittance of the z-scan is given by [15]:

$$T = \left[1 + \frac{\theta_A}{2}\tan^{-1}\left(\frac{2x}{3+x^2}\right)\right]^2 + \left[\frac{\theta_A}{4}\ln\left(\frac{1+x^2}{9+x^2}\right)\right]^2 \quad (5)$$

where θ_A is the fitting parameter (for us) and $x = z/z_0$. As in the previous model, this expression is valid for steady-state conditions. The model of reference [13] does not allow to obtain an analytic expression for the normalized transmittance. Then, it is possible to show the calculated curve for a value of the m parameter and for a given value of the on-axis nonlinear phase shift $\Delta\Phi_0$. In this case, we have two fitting parameters.

First, the fitting for the smaller amplitude experimental curve (2.5 mW of incident power) is presented in Figure 5. As reference, we present here, the z-scan curve obtained with the local model (grey line) of Sheik-Bahae [5], where a $\Delta\Phi_0 = -0.2\pi$ rad was used. The dashed line corresponds to the thermal lens model, where a value of $\theta_{TL} = 0.04\pi$ rad was used in Equation (4). The dotted line corresponds to the aberrant thermal lens model, where a value of $\theta_A = 0.08\pi$ rad was used in Equation (5). The solid black line corresponds to the nonlocal model [13] with $m = 0.4$ and $\Delta\Phi_0 = -0.18\pi$ rad. We can observe that the models that present remarkable differences with the experimental results are the local models of Sheik-Bahae and the aberrant thermal lens model, in fact, this last model predicts a different position of the peak and the valley. The thermal lens and the nonlocal models follow with good correspondence; the experimental results.

In Figure 6, we show the fittings of the experimental data for an incident power of 40 mW. For this experimental curve, it was not possible to obtain a good fitting

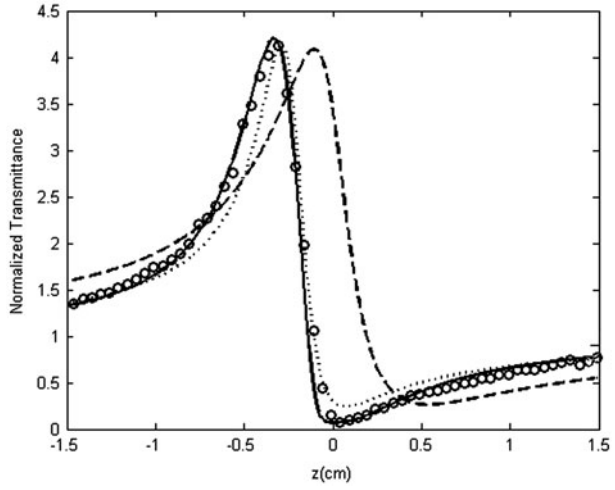

Figure 6. Experimental (o) and calculated z-scan curves for the F sample with an incident power of 40 mW. Fitting with: thermal lens model (dashed line) with $\theta_{TL} = -0.5\pi$ rad; aberrant thermal lens model (dotted line) with $\theta_A = -0.9\pi$ rad and nonlocal model (black solid line) of reference [13] with $m = 0.4$ and 2.9π rad.

with the local model of Sheik-Bahae. The dashed line corresponds to the thermal lens model, with $\theta_{TL} = 0.5\pi$ rad. The dotted line corresponds to the aberrant thermal lens model, with $\theta_A = 0.9\pi$ rad. The solid line corresponds to the nonlocal model, with $m = 0.4$ and $\Delta\Phi_0 = -2.9\pi$ rad. We can observe that the aberrant thermal lens model gave the major differences with the experimental data. The thermal lens model and the nonlocal model follow with good correspondence; the experimental curve. However, only in the nonlocal model, the increasing of the fitting parameter ($\Delta\Phi_0$) was in the same rate as the incident power. In Figure 7, we show the fitting of the experimental results, for the rest of the powers, with the nonlocal model.

In Figure 8, we show the fitting with the nonlocal model of the experimental z-scan curves obtained with an incident power of 16 mW for samples with different concentrations of CTAC. The nonlocal z-scan curves were numerically calculated with $m = 0.4$ and $\Delta\Phi_0$ of: -0.3π rad for B sample (+), -0.75π rad for C sample (o), -0.9π rad for D sample (×), -1.1π rad for E sample (□) and -1.25π rad for F sample (*). As can be seen, the amplitude of the z-scan curves increases as the concentration of CTAC and Δz_{p-v} is almost the same for all the curves. It is important to note that the numerically calculated curves not only reproduce the amplitude and position of the peak and valley of the experimental curves, they accurately reproduce the transmittance data far from the beam waist.

The value of the m parameter to fit the experimental results was 0.4. This means that phase changes, Equation (2), take the following form:

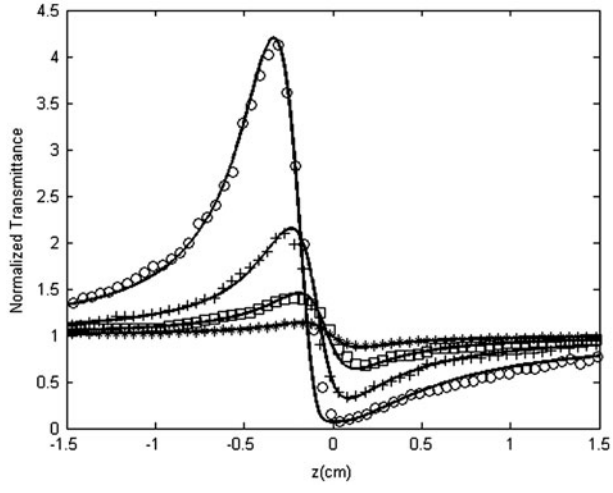

Figure 7. Experimental (symbol) and numerically calculated (lines) z-scan curves for the F sample. The black solid lines were obtained with $m = 0.4$ and $\Delta\Phi_0$ of: -0.18π rad for 2.5 mW (*), -0.55π rad for 8 mW (□), -1.25π rad for 16 mW (+) and -2.9π rad for 40 mW(o).

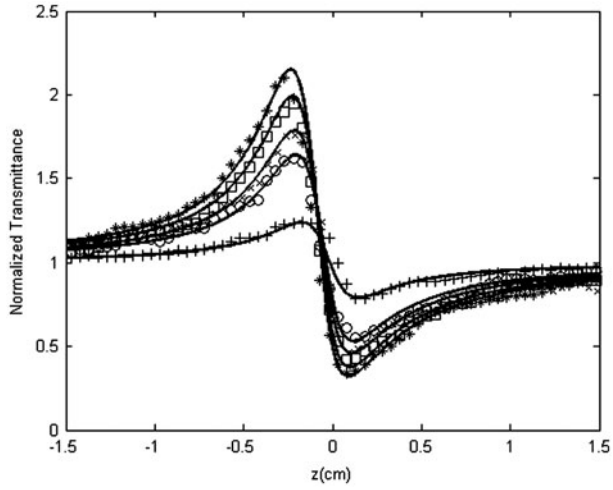

Figure 8. Experimental (symbol) and numerically calculated (lines) z-scan curves for an incident power of 16 mW and samples with different CTAC concentrations. The black solid lines were obtained with $m = 0.4$ and $\Delta\Phi_0$ of: -0.3π rad for B (+), -0.75π rad for C (o), -0.9π rad for D (×), -1.1π rad for E (□) and -1.25π rad for F (*) samples.

$$\Delta\phi(r) = \frac{\Delta\Phi_0}{[1 + (z/z_0)]^{0.4/2}} \exp\left(-\frac{2r^2}{\left(\frac{w}{\sqrt{0.4/2}}\right)^2}\right) \quad (6)$$

This means that the phase change is also Gaussian but with a radius 2.23 times bigger than that of the incident beam.

6. Conclusions

We investigated the nonlocality in the nonlinear refractive index response of colloidal suspensions of gold nanoparticles. In the synthesis of gold nanoparticles, the use of the CTAC surfactant agent allows to control the size of the nanoparticles between 25 and 50 nm, and consequently the nonlinear optical response. Experimental closed-aperture z-scan curves under CW illumination were obtained. The results demonstrate a negative nonlinear refractive index and that the amplitude of the z-scan curves grows with the CTAC concentration. Different models were used to fit the experimental data, obtaining that the phenomenological nonlocal model of reference [13] gave the better agreement when the m parameter was equal to 0.4. This means that the phase changes extend more than two times the size of the incident beam.

Funding

This work was partially supported by PROMEP, SEP, México; A. Balbuena Ortega acknowledges grant receipt of CONACYT, México.

References

[1] Daniel, M.C.; Astruc, D. *Chem. Rev.* **2004,** *104,* 293–346.

[2] Hari, M.; Joseph, S.A.; Balan, N.; Mathews, S.; Kumar, R.; Mishra, G.; Yadhav, R.R.; Radhakrishnan P.; Nampoori V.P.N. *J. Nonlinear Optic. Phys. Mater.* **2011,** *20,* 467–475.

[3] Feifei, C.; Shixun, D.; Tiefeng, X.; Xiang, S.; Changgui, L.; Qiuhua, N.; Chao, L.; Jong, H. *Chem. Phys. Lett.* **2011,** *514,* 79–82.

[4] Torres-Torres, C.; Castro-Chacón, J.H.; Castañeda, L.; Rangel Rojo, R.; Torres-Martínez, R.; Tamayo-Rivera, L.; Khomenko, A.V. *Opt. Express* **2011,** *19,* 16346–16355.

[5] Sheik-Bahae, M.; Said, A.A.; Van Stryland, E.W. *Opt. Lett.* **1989,** *14,* 955–957.

[6] Sheik-Bahae, M.; Said, A.A.; Wei, T.H.; Hagan, D.J.; Van Stryland, E.W. *IEEE J. Quant. Electron.* **1990,** *26,* 760–769.

[7] Karimzadeh, R.; Nastaran, M. *Phys. Stat. Sol. (b)* **2010,** 247*,* 365–370.

[8] Cuppo, F.L.S.; Neto, A.M.F.; Gómez, S.L. *J. Opt. Soc. Am. B* **2002,** *19,* 1342–1348.

[9] Karimzadeh, R.; Nastaran, M. *Opt. Laser Technol.* **2010,** *42,* 783–789.

[10] Sheldon, S.J.; Knight, L.V.; Thorne, J.M. *Appl. Opt.* **1982,** *21,* 1663–1669.

[11] Zamir Anvari, J.; Karimzadeh, R.; Mansour, N. *J. Opt.* **2010,** *12,* 035212.

[12] Pálfalvi, L.; Tóth, B.C.; Almási, G.; Fülöp, J.A.; Hebling, J. *Appl. Phys. B* **2009,** *97,* 679–685.

[13] García Ramírez, E.V.; Arroyo Carrasco, M.L.; Méndez Otero, M.M.; Reynoso Lara, E.; Chávez-Cerda, S.; Iturbe Castillo, M.D. *J. Opt.* **2011,** *13,* 085203.

[14] García Ramírez; E.V.; Arroyo Carrasco, M.L.; Méndez Otero, M.M.; Chávez-Cerda, S.; Iturbe Castillo, M.D. *Opt. Express* **2010,** *18,* 22067–22079.

[15] Carter, C.A.; Harris, J.M. *Appl. Opt.* **1984,** *23,* 476–481.

[16] Luty-Błocho, M.; Fitzner, K.; Hessel, V.; Löb, P.; Maskos, M.; Metzke, D.; Pacławski, K.; Wojnicki, M. *Chem. Eng. J.* **2011,** *171,* 279–290.

[17] Qin, Y.; Ji, X.; Jing, J.; Liu, H.; Wu, H.; Yang, W. *Colloids Surf., A* **2010,** *372,* 172–176.

[18] Pálfalvi, L.; Hebling, J. *Appl. Phys. B* **2004,** *78,* 775–780.